Prediction of fluid slip in cylindrical nanopores using equilibrium molecular simulations

Sam, Alan; Hartkamp, Remco; Kannam, Sridhar Kumar; Sathian, Sarith P.

Important note
To cite this publication, please use the final published version (if applicable).
Please check the document version above.

PAPER

Prediction of fluid slip in cylindrical nanopores using equilibrium molecular simulations

To cite this article: Alan Sam *et al* 2018 *Nanotechnology* **29** 485404

View the article online for updates and enhancements.

Prediction of fluid slip in cylindrical nanopores using equilibrium molecular simulations

Alan Sam[1], Remco Hartkamp[2], Sridhar Kumar Kannam[3,4] and Sarith P Sathian [1,5]

[1] Department of Applied Mechanics, Indian Institute of Technology Madras, Chennai, India
[2] Process & Energy Department, Delft University of Technology, Leeghwaterstraat 39, 2628 CB Delft, The Netherlands
[3] Faculty of Science, Engineering and Technology, Swinburne University of Technology, Melbourne, Victoria 3122, Australia
[4] School of Applied Sciences, RMIT University, Melbourne, Victoria 3001, Australia

E-mail: alansarun@gmail.com, r.m.hartkamp@tudelft.nl, urssrisri@gmail.com and sarith@iitm.ac.in

CrossMark

Abstract

We introduce an analytical method to predict the slip length (L_s) in cylindrical nanopores using equilibrium molecular dynamics (EMD) simulations, following the approach proposed by Sokhan and Quirke for planar channels [39]. Using this approach, we determined the slip length of water in carbon nanotubes (CNTs) of various diameters. The slip length predicted from our method shows excellent agreement with the results obtained from nonequilibrium molecular dynamics (NEMD) simulations. The data show a monotonically decreasing slip length with an increasing nanotube diameter. The proposed EMD method can be used to precisely estimate slip length in high slip cylindrical systems, whereas, L_s calculated from NEMD is highly sensitive to the velocity profile and may cause large statistical errors due to large velocity slip at the channel surface. We also demonstrated the validity of the EMD method in a BNNT-water system, where the slip length is very small compared to that in a CNT pore of similar diameter. The developed method enables us to calculate the interfacial friction coefficient directly from EMD simulations, while friction can be estimated using NEMD by performing simulations at various external driving forces, thereby increasing the overall computational time. The EMD analysis revealed a curvature dependence in the friction coefficient, which induces the slip length dependency on the tube diameter. Conversely, in flat graphene nanopores, both L_s and friction coefficient show no strong dependency on the channel width.

Keywords: slip length, carbon nanotube, molecular dynamics, nanofluidics

(Some figures may appear in colour only in the online journal)

1. Introduction

Nanofluidics [1], the study of fluid flow in systems with nanometric sizes, has important applications in numerous fields of study, such as engineering, biology, physics, chemistry, and medicine [2]. For example, the ultra-fast water flow through graphitic nanoconduits, such as graphene and carbon nanotubes (CNTs), shows huge potential for development of membranes for applications such as water desalination, ultrafiltration, gas separation, and energy storage [3]. Fluids confined in a nanoscale domain exhibit distinctive structural and dynamic properties that deviate from macroscopic fluid dynamics [1, 4, 5]. The small number of confined molecules at the nanoscale is insufficient to represent a macroscopically small volume with homogeneous properties. Consequently, continuum hydrodynamics theory with the

---

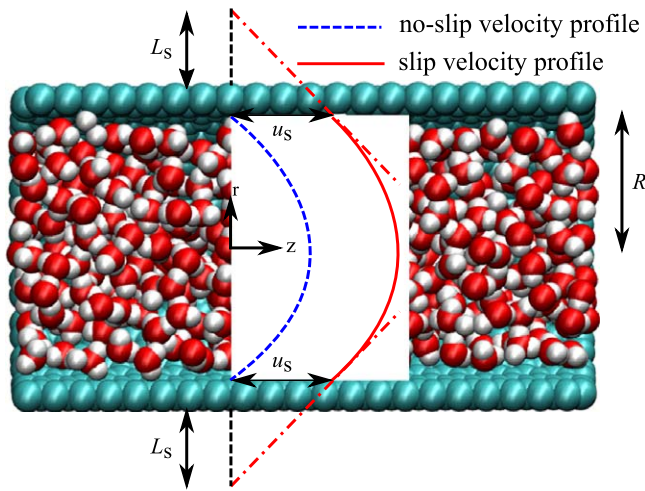[5] Author to whom any correspondence should be addressed.

Figure 1. Schematic depiction of velocity profiles of water flow through carbon nanotubes with and without boundary slip. L_s characterizes the fluid-solid interfacial slip.

assumption of zero relative fluid velocity at the fluid-solid interface (known as the no-slip boundary condition) may not apply at nanometer length scales [6, 7]. At these scales, fluid flow is characterized by a velocity slip. This applies especially to hydrophobic channels, although recent study showed that the slip can also be significant on hydrophilic surfaces [8]. Whereas understanding and predicting of slip in nanochannels is pivotal for the development of nanofluidic devices, measurements and simulations have thus far not been able to provide a consistent view of the amount of slip at given surfaces.

Over the past centuries, many researchers have put forward theories to accurately formulate the boundary condition at a fluid-solid interface. Among them, the kinetic theory based tangential momentum accommodation coefficient model by Maxwell [9] and the Navier-slip model provide much insight on the molecular interactions at the surface. Navier [10] proposed a general boundary condition where the slip behavior is characterized by a slip length (L_s), defined as:

$$L_s = \frac{\eta}{\lambda},$$ (1)

where η is the fluid shear viscosity and λ is the interfacial friction coefficient at the fluid-solid interface. L_s represents the distance from the wall at which the fluid boundary slip velocity (u_s) equals the wall velocity, see figure 1. L_s is negligible relative to the flow domain size in macroscale channels, but becomes significant as the channel size reduces to a few molecular diameters. Due to their high surface-to-volume ratio, the flow through nanochannels strongly depends on the nature of the interacting solid. For example, slip lengths of water in hydrophobic carbon nanostructures, such as graphene slit pores and CNTs, greatly exceed typically pore dimensions [11–24], whereas the slip length of water is small in boron nitride nanopores [24]. In addition to the influence of the material, L_s also shows a dependency on the channel geometry. For example, in cylindrical nanopores L_s varies with the tube diameter due to the effect of curvature [17, 19]. In such systems,

the surface potential energy landscape becomes smoother as the tube diameter decreases. This facilitates an almost frictionless fluid transport through the nanotube. Curvature and confinement effects diminish upon increasing the tube diameter, such that L_s converges towards values corresponding to a slit pore, for which the slip length is independent of the pore width [21, 23].

Ever since Hummer *et al* [15] observed the spontaneous and fast filling of CNTs immersed in water, much attention has been focussed on developing methods predicting the slip length and flow rate in these hydrophobic graphitic conduits [25, 26]. The large slip lengths of water in CNTs suggest an almost negligible solid–liquid interfacial friction, which leads to rapid fluid transport [7, 20–22, 27]. However, the magnitude of L_s and flow rate obtained from various experimental and computational studies are widely scattered, which may hinder its utility for commercial purposes. Slip lengths of 1–500 000 nm have been reported for CNTs of 0.8–10 nm in diameter. Many authors reported a monotonically decreasing L_s with tube diameter [18, 21–24, 28], while others observed the opposite trend, suggesting a reduced interfacial friction with increasing diameter [16, 29, 30].

The observed discrepancies among the experimental studies can be attributed to defects in the tube and to the inaccurate estimation of the tube diameter, which may also correspond to the average of a pore size distribution. Moreover, evaluation of L_s requires atomic-scale resolution, which is difficult to achieve in experiments. Conversely, molecular dynamics (MD) simulations provide the opportunity to predict slip lengths in well-defined geometries and gain insight into the molecular mechanism underlying slip behavior. Nevertheless, similar to the experimental literature, also the slip lengths computed using MD are scattered among various studies, owing to differences in methodology and force fields used. For instance, in MD, the slip length can be estimated using equilibrium or nonequilibrium methods. In nonequilibrium MD (NEMD), the fluid is driven through the tube by an external driving force and L_s and slip velocity (relative fluid velocity at the wall) can be determined directly from the resulting streaming velocity profile (figure 1). In NEMD simulation of a high slip system, such as water in a graphitic nanopore, it is challenging to accurately obtain the slip length. Due to the large slip velocity, the calculated slip length is highly sensitive to the velocity gradient at the surface.

To collect sufficient statistics despite the small systems and short simulation time compared to those considered in experiments, external driving forces applied in NEMD simulations are typically several orders of magnitude larger than the accessible driving forces in experiments [31]. It is therefore important to validate that the fluid response resides in the linear velocity response regime, such that results can be extrapolated down to experimental conditions. The linear regime can be identified by performing NEMD simulations at multiple external forces. In the linear regime, L_s is independent of the driving force (since the slip velocity and the curvature of the velocity profile both increase linearly with the driving force), but increases rapidly with the driving forces beyond the linear regime.

In equilibrium MD (EMD), following the boundary slip expression by Navier (see equation (1)), L_s can be determined

by calculating the interfacial friction [32–38]. An alternative method using EMD is to determine the relaxation time from the exponential fit of the collective velocity autocorrelation function (VACF). For a planar channel, Sokhan and Quirke derived an equation in which, L_s can be estimated directly using the relaxation time [39–41]. These EMD approaches enable us to predict the slip length from a single EMD simulation. Besides the advantage that there is no need in EMD to identify the linear regime, it also has been found that the EMD methods are more reliable for estimating L_s compared to the NEMD approach, even for a high slip system [36].

While slip lengths for fluid flow along a planar wall can be directly calculated using the relaxation time in EMD simulations, an equivalent approach does not exist for cylindrical pores, which occur throughout nature and industry. In this study, following the approach of Sokhan and Quirke on a planar geometry [39], we derived an expression for L_s in cylindrical channels as a function of relaxation time. The method is validated on a CNT-water system since it offers a wide range of interesting applications. Furthermore, a boron nitride nanotube (BNNT) filled with water has been considered, to validate the method also for a more hydrophilic surface. The results obtained from the EMD approach are compared to the results from NEMD simulations in which the fluid is subjected to a Poiseuille flow. To investigate the effects of curvature on the fluid transport, we also simulated flow of water in planar graphene channels. The data for slip length in CNTs were compared against the simulations for graphene nanopores, where the observed slip depends only on the pore width and external acceleration.

2. Methods

2.1. Theory

Consider a fluid confined in a cylindrical tube of radius R and surface area A_{surf}. We assume fluid flow along the z-direction (CNT axis). The collective motion u of the fluid of mass M in the tube can be described by the Langevin equation for the Brownian motion [40, 42]. The time rate of change of the total momentum of the fluid in the flow direction is balanced by the sum of forces due to fluid viscosity (viscous frictional force) and momentum transfer in molecular collisions with the wall (random force):

$$M\frac{\partial u(t)}{\partial t} = -\lambda u(t) + \zeta(t),\qquad(2)$$

where the viscous frictional force is proportional to the collective velocity of fluid $u(t)$, and λ is the (Stokesian) friction coefficient. In the heavy mass limit of the Brownian particle, the random force ($\zeta(t)$) reduces to a Markovian noise with zero first moment, $\langle\zeta(t)\rangle = 0$, and strength proportional to the friction coefficient, $\langle\zeta(t_1)\zeta(t_2)\rangle = 2\lambda k_B T\delta(t_1 - t_2)$. Multiplying both sides of the equation (2) by $u(0)$ and applying the heavy mass approximation, we obtain:

$$M\frac{\partial C_c(t)}{\partial t} = -\lambda C_c(t).\qquad(3)$$

$C_c(t)$ relates to the streaming of fluid in the pore, which is written in terms of the center of mass velocity ($u(t)$):

$$C_c(t) = \langle u(t)u(0)\rangle.\qquad(4)$$

Equation (3) has a solution:

$$C_c(t) = \frac{k_B T}{M}\exp\left(-\frac{t}{\tau}\right).\qquad(5)$$

Thus, the center of mass VACF ($C_c(t)$) decays exponentially with time, where the static limit ($C_c(0)$) is proportional to the temperature (T) and k_B is the Boltzmann constant. The relaxation time τ of $C_c(t)$ is related to the interfacial friction coefficient (λ), by:

$$\lambda = \frac{M}{\tau}.\qquad(6)$$

At any finite temperature (T), the fluid exerts a tangential force (or Stokesian drag) F_s on the wall, causing a shear stress on the tube surface. Under the heavy mass approximation, we obtain the wall shear stress (σ_{rz}), given by:

$$\sigma_{rz} = -\frac{F_s}{A_{surf}} = \frac{Mu}{A_{surf}\tau} \equiv \frac{\rho Ru}{2\tau},\qquad(7)$$

where u is the mean velocity of the fluid of density ρ (assumed to be constant).

The Stokesian drag force per unit area exerted on the wall can be equated in terms of the total external force acting on the fluid particles [39, 43]. Applying the linear momentum balance, the wall shear stress can also be written in terms of the external acceleration (g) acting on the fluid:

$$\frac{1}{r}\frac{d}{dr}(r\sigma_{rz}(r)) = \rho g\qquad(8)$$

such that, under the assumption of uniform density, the wall shear stress can be written as:

$$\sigma_{rz} = \frac{R\rho g}{2}.\qquad(9)$$

Combining equations (7) and (9), the average fluid velocity in the pore:

$$u = \tau g.\qquad(10)$$

For a Newtonian fluid of viscosity η, the shear stress is linearly related to the gradient of the velocity [4]. An expression for the radial velocity profile ($u_z(r)$) can be derived by substituting the Newtonian constitutive relation into equation (8):

$$\frac{1}{r}\frac{d}{dr}\left(r\frac{du_z}{dr}\right) = -\frac{\rho g}{\eta}.\qquad(11)$$

Assuming the velocity to be symmetric about the tube center (at $r = 0$; $du_z/dr = 0$), and applying the slip boundary condition at the tube wall ($u_z(r = R) = u_s$), we obtain the following quadratic velocity profile:

$$u_z(r) = \frac{\rho g}{4\eta}(R^2 - r^2) + u_s.\qquad(12)$$

The mean fluid velocity can be calculated by averaging equation (12) over the tube area:

$$u = \frac{1}{R^2} \int_0^R 2r u_z(r)\, dr, \tag{13}$$

$$= \frac{1}{R^2} \left[\frac{\rho g}{2\eta} \left(\frac{1}{2} r^2 R^2 - \frac{1}{4} r^4 \right) + r^2 u_s \right]_0^R \tag{14}$$

$$= \frac{\rho g}{2\eta} \left(\frac{1}{2} R^2 - \frac{1}{4} R^2 \right) + u_s. \tag{15}$$

Combining equations (10) and (15), we obtain the predicted slip velocity:

$$u_s = \tau g - \frac{\rho g R^2}{8\eta}. \tag{16}$$

Substituting equation (16) into equation (12) gives the total velocity profile:

$$u_z(r) = \frac{\rho g}{4\eta} \left(\frac{R^2}{2} - r^2 \right) + \tau g. \tag{17}$$

Finally, the slip length can be calculated via:

$$L_s = \left(\frac{du_z}{dr} \Big|_{r=R} \right)^{-1} u_s \tag{18}$$

$$= \left(\frac{\rho g R}{2\eta} \right)^{-1} \left(\tau g - \frac{\rho g R^2}{8\eta} \right) \tag{19}$$

$$= \frac{2\eta\tau}{\rho R} - \frac{R}{4}. \tag{20}$$

Equation (20) shows L_s in terms of relaxation time (τ) and exhibits a nonlinear dependence on the pore size. Note that the resulting slip length is independent of the external driving force. Sokhan and Quirke established a similar relationship, for planar Poiseuille flow in a channel of $2h$ wide: [39]

$$L_s = \frac{\eta\tau}{\rho h} - \frac{h}{3}. \tag{21}$$

2.2. Simulation system

We simulated armchair CNTs ($n = m$) of chiralities $n = 10$, 12, 14, 16, 18, 20, 24, 28, 32 and 36, having diameters ranging from 1.36 to 4.88 nm and length 5 nm. A 5 nm long armchair BNNT of chirality $n = 36$, was also considered. The diameter of both CNT and BNNT pores was calculated using the equation, $d = \sqrt{3}\, l / \pi \sqrt{n^2 + nm + m^2}$, where the bond length (l) in CNT and BNNT was 0.142 and 0.145 nm, respectively. We also simulated planar graphene channels having x and y dimensions of 4 nm each and a pore width in the range of 1–5 nm. To obtain the correct water density inside the channels, we immersed the channels in a large water bath, allowing water to fill the tubes at 298 K temperature and 1 atm pressure. After 1 ns equilibration, we removed water outside the channels and applied periodic boundary conditions along the directions where the flow is

unrestricted (i.e., z-axis for the cylindrical pores and x and y-axes for graphene channel). In all other directions we applied nonperiodic boundary condition. Using these equilibrated simulation systems as the starting configuration, we performed EMD and NEMD simulations in the NVT ensemble at 298 K. The system temperature was controlled by applying the Nosé–Hoover thermostat [44] to the wall. A recent study by Sam *et al* [28] demonstrated the influence of tube flexibility on the confined fluid transport. The systems were initially equilibrated for 20 ns long. In NEMD, the equilibration is monitored by using the development of the streaming velocity profiles in time. For each configuration, 10 independent simulations with different initial randomized velocities were carried out for 20 ns each to collect adequate statistics.

Carbon–carbon interactions were modeled with the reactive empirical bond order potential [45], which has been widely used to study graphene and CNTs. Water was modeled with the SPC/E model, whose transport properties agree well with experiments [46, 47]. Fluid-wall Lennard-Jones (LJ) interaction parameters were taken from Werder *et al* [48]. Both the fluid–fluid and fluid-solid LJ interactions were truncated at a distance of 1 nm. Long-range electrostatic interactions were computed using the Wolf summation method, with a cut-off distance of 1 nm and a damping parameter of 2.25 nm^{-1} [49].

BNNT was modeled using the Tersoff potential [50, 51]. The partial charges of boron and nitrogen atoms in BNNT were 0.35e and $-0.35e$, respectively. The parameters of the LJ potential describing the van der Waals interactions between water and BNNT were obtained using the Lorentz–Berthelot mixing rule [52]. All the simulations reported here were carried out using the LAMMPS package [53], with a time step of 2 fs.

EMD simulations were performed on both cylindrical (water-CNT and water-BNNT) and planar systems (water-graphene) and L_s was calculated using equations (20) and (21), respectively. We fitted the collective VACF using an exponential function to estimate the relaxation time in both planar and cylindrical channels. L_s was predicted for the independent simulations and we performed averaging and error analysis using the variations in slip lengths obtained from the 10 independent simulations. Furthermore, we used the shear viscosity of bulk SPC/E water (7.04×10^{-4} Pa s) [54], for determining the slip length for all the nanopore and nanochannels used in this study. For very narrow pores (<1 nm) the viscosity is known to become nonlocal and methods such as Green–Kubo fails. However, previous studies have reported that the shear viscosity of water maintains its bulk value down to confinements of ≈ 1 nm [7, 55]. It should also be noted that the dependency of L_s on the fluid viscosity (η) obtained from EMD (equation (20)) and NEMD (combining equations (12) and (18)) is the same. Therefore, assuming bulk water viscosity to calculate L_s does not have a significant effect on the comparison of slip lengths between both methods.

In NEMD, a gravity-like acceleration in the range 0.5–10×10^{11} m s^{-2} was applied to each water molecule to
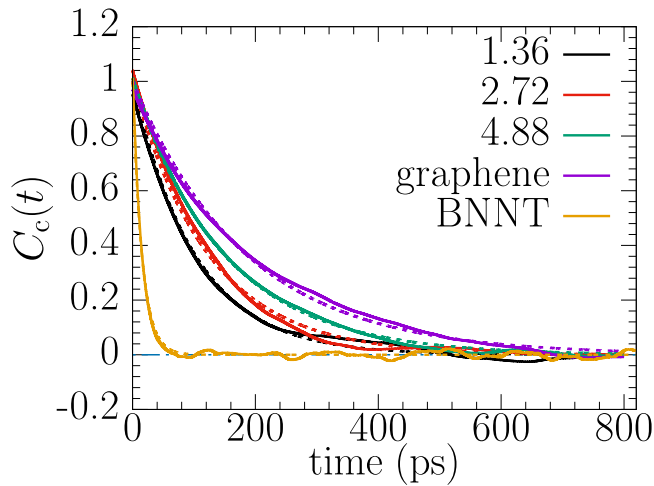
Figure 2. Normalized collective velocity autocorrelation function and corresponding fit from EMD simulations for 1.36, 2.72 and 4.88 nm diameter CNTs, a BNNT of 4.98 nm diameter and 5 nm graphene slit pore.
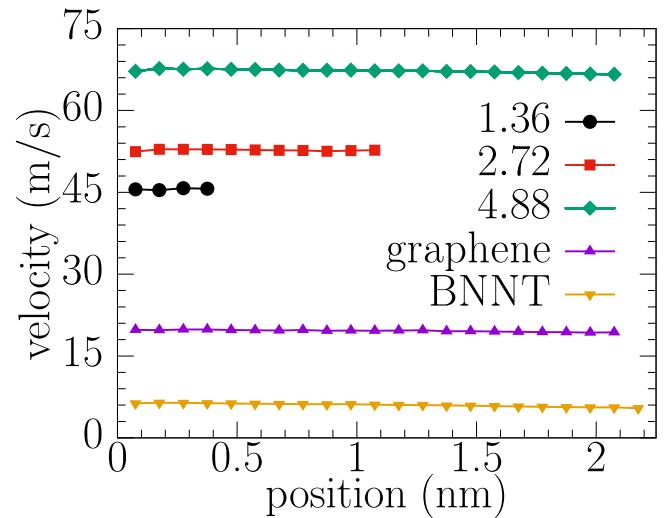

Figure 3. Velocity profiles of water at various positions from NEMD simulation for 1.36, 2.72 and 4.88 nm diameter CNTs, a BNNT of 4.98 nm diameter and 5 nm graphene slit pore. NEMD data are obtained at an external acceleration of 4×10^{11} m s^{-2} for CNTs and at 1×10^{11} m s^{-2} for graphene channels.

generate Poiseuille flow. This range was chosen to identify the linear response regime, in which the slip length is independent of the external acceleration. The streaming velocities in CNTs and BNNT were fitted to a quadratic equation, $u_z = ar^2 + b$ (for plane Poiseuille flow, $u_x = az^2 + b$). Parameters a and b were constrained using equation (12), such that they satisfy the shear viscosity and density of the bulk fluid. From these fits and NEMD velocity profiles, L_s was predicted using equation (18).

3. Results and discussions

We first investigate the relaxation of the normalized collective VACF $C_c(t)$ calculated using the z component of the center of mass velocities in EMD (equation (4)). Figure 2 shows $C_c(t)$ profiles and their corresponding exponential fits (equation (5)) for CNTs having diameter 1.36, 2.72 and 4.88 nm, a BNNT of diameter 4.98 and a 5 nm graphene slit pore. Using the relaxation times τ obtained from the fitted correlation functions, we calculated the mean velocity, slip length and interfacial friction coefficient of water flow in all CNT, BNNT and graphene channel widths. NEMD analysis of the water flow in CNTs and graphene shows plug-like streaming velocity profiles; i.e. the variation in the velocity from the center to the channel wall is negligibly small (shown in figure 3). Since the velocity profiles were plug-like, we take the slip velocity as the average streaming velocity of the fluid for estimating the slip velocity. While in BNNT, the streaming velocity varies slightly from the plug profile (not clearly visible because of the large scale used in figure 3). Therefore, to calculate L_s, we take the velocity of the water layer adjacent to the solid boundary as the slip velocity.

3.1. CNT-water system

Figure 4(a) shows the average fluid velocities as a function of the tube diameter calculated using equation (10). The

NEMD results correspond to an external acceleration of 4×10^{11} m s^{-2}. For both methods, the average fluid velocity increases nonmonotonically with the tube diameter. The water molecules slip past the tube at higher velocities than predicted using the Hagen–Poiseuille equation with the no-slip boundary condition (see figure 4(a)). The no-slip velocity varies quadratically with the tube diameter. However, the values are negligible when compared to the slip velocities, with the smallest and highest diameter channels having velocities 0.026 m s^{-1} and 0.334 m s^{-1}, respectively. Earlier studies have attributed the enhanced fluid velocities in CNTs to the smooth surface potential energy landscape, causing the fluid to experience minimal frictional resistance [21]. Figure 4(b) shows the mean fluid velocity as a function of the external acceleration in a 2.72 nm diameter CNT. Equation (10) shows a simple linear relationship between the average fluid velocity and the external acceleration. In the lower regime of the accelerations applied to the fluid in NEMD, the mean velocity varies linearly and is significantly lower than the molecular thermal velocity ($\approx$340 m s^{-1}) at 298 K. Consequently, the velocities can be extrapolated down to the experimental ranges to accurately estimate the slip length.

Figure 5 shows variation of L_s with the nanotube diameter calculated from both EMD and NEMD simulations. NEMD data are obtained at an external acceleration 4×10^{11} m s^{-2}. The applied acceleration is in the linear regime for a CNT of 2.72 nm in diameter and was used for the estimation of slip length in all the tubes. Following the EMD approach, we found that L_s decreases from 230 to 90 nm as the nanotube diameter increases from 1.36 to 4.88 nm. The slip length may decrease even further for wider tubes and attain a magnitude equivalent to that in a planar graphene nanopore. The predicted values from our approach agree with the NEMD data. The results are also in good agreement with
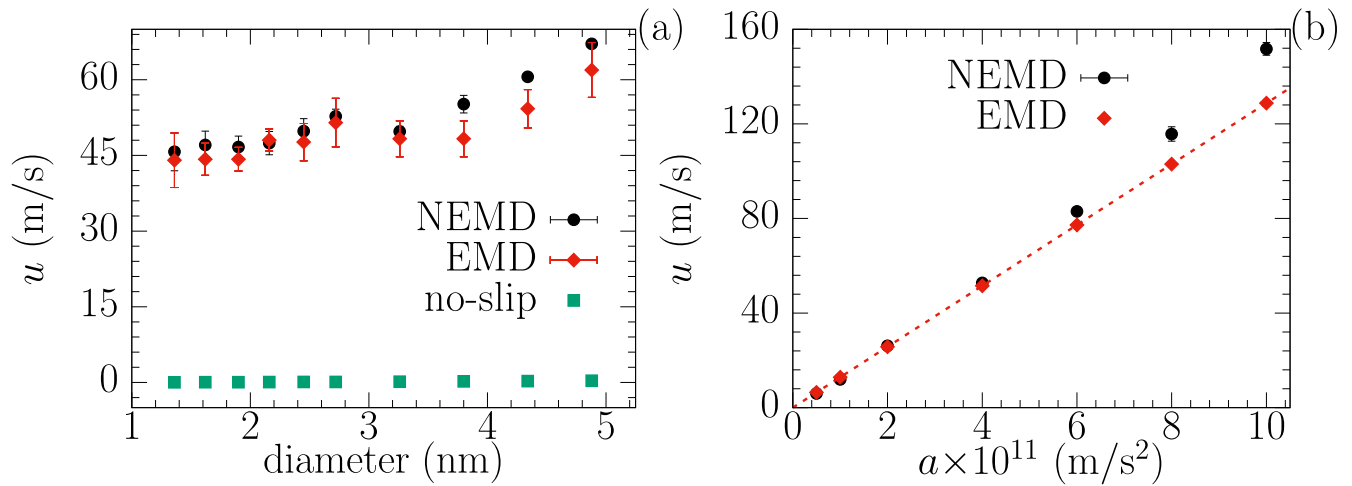
Figure 4. (a) Average fluid velocity as a function of the nanotube diameter from EMD and NEMD simulations. NEMD data are obtained at an external acceleration 4×10^{11} m s^{-2}. The average velocities calculated using Hagen–Poiseuille formalism with no-slip boundary condition are also shown. (b) Average fluid velocity with external acceleration for tube diameter 2.72 nm. The dotted straight line is prediction from EMD. The error bars show the standard error.
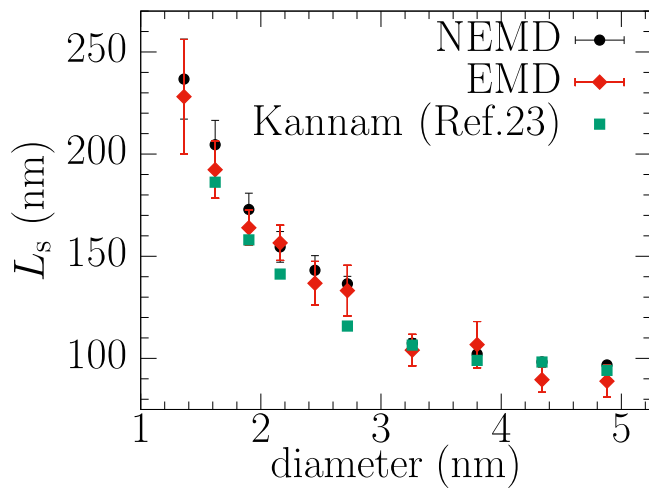

Figure 5. Slip length as a function of the nanotube diameter from EMD and NEMD simulations. NEMD data are obtained at an external acceleration 4×10^{11} m s^{-2}.

the results of Kannam *et al* [23]. However, as mentioned previously, the magnitude of L_s is largely scattered among the simulation literature. The discrepancy could be due to the following reasons: (a) The water density inside the tubes depends on the CNT diameter in our simulations [28], while in many other simulation studies the tubes are filled with water at bulk density. We found that the effect of this methodological difference is significantly higher in smaller diameter tubes ($\sim$30% difference in L_s for the lowest diameter). (b) The potentials used to model the interatomic interactions of water and CNTs varied between studies [23, 56]. (c) Previous studies on water transport through CNTs kept the solid atoms fixed to their lattice sites while thermostatting the fluid [16, 18, 20–22, 57–59], thereby lowering the computational cost. However, recent studies have reported that the internal dynamics (wall–wall interactions) of the solid atoms significantly influences the fluid boundary slip [28, 60, 61]. We performed simulations in

which the thermostat was applied to the flexible tube walls and found the slip length up to 20% higher compared to that in the rigid CNTs.

3.2. BNNT-water system

Unlike the very large slip of water in CNTs, many other fluid-solid interfaces are characterized by smaller slip lengths and velocities at the solid surface. To demonstrate the validity of equation (20) for such cases, we simulated water flow in a BNNT, in which the fluid slippage at the solid boundary is expected to be very small compared to that in CNTs [24]. Recent investigations have revealed that the friction coefficient of water at the BNNT surface is extremely large due to the presence of strong electrostatic interactions between the water molecules and the partial charges on BNNT atoms, causing very low slip [52]. We performed both EMD and NEMD simulations to calculate the slip length in a BNNT of diameter 4.98 nm. From the EMD method, we found that the L_s of water in a BNNT is $\approx$8 nm, which is approximately 10 times lower than the slip length in a similar diameter CNT. The results show excellent agreement with the results from NEMD simulations (<5% difference in the value of L_s), where the fluid is subjected to an external acceleration 4×10^{11} m s^{-2}. The slip velocity of water in a BNNT was very small, as opposed to the very large velocities of water at the CNT surface (figure 3). We thus demonstrated the applicability of the proposed EMD approach to determine the slip length in systems of different boundary conditions.

3.3. Graphene-water system

Figure 6 shows the mean streaming velocity of water in a planar graphene channel as a function of (a) width and (b) external acceleration. In EMD, the average velocity is obtained from the relaxation time using equation (10). Figure 6(a) shows a continuous increase in the average velocity with increasing pore width. The corresponding
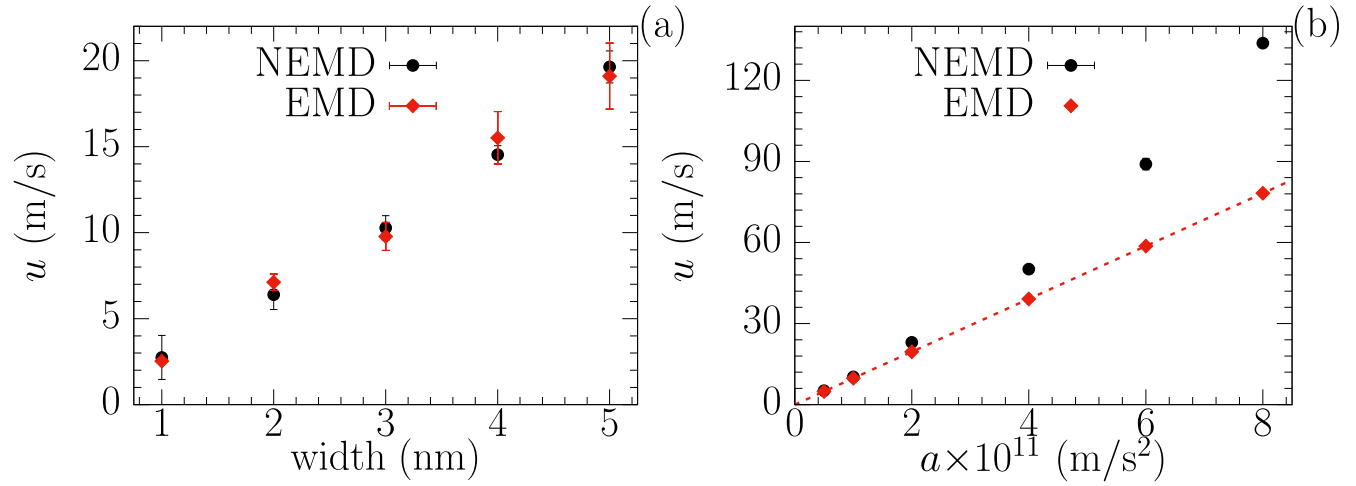
Figure 6. (a) Average fluid velocity as a function of the pore width from EMD and NEMD simulations. NEMD data are obtained at an external acceleration 1×10^{11} m s^{-2}. (b) Average fluid velocity with external acceleration for pore width 3 nm. The dotted straight line is prediction from EMD. The error bars show the standard error.
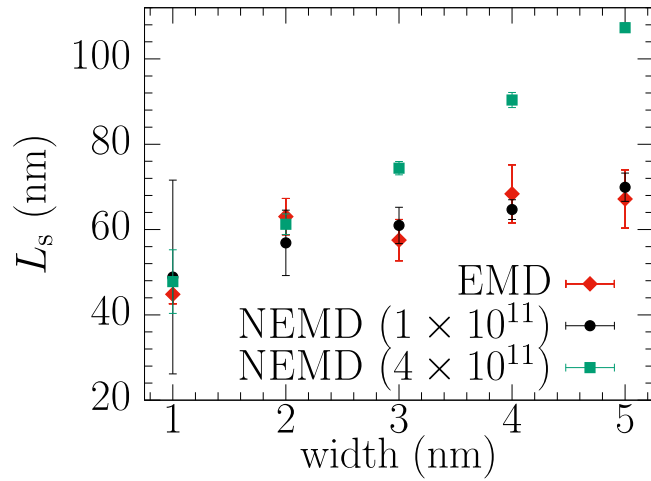

Figure 7. Slip length of water in graphene channel as a function of the pore width from EMD and NEMD simulations. NEMD data are obtained at external accelerations 1×10^{11} and 4×10^{11} m s^{-2}.
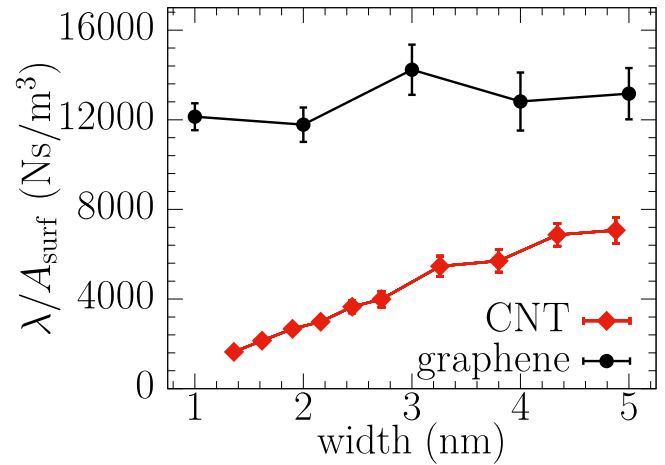

Figure 8. The interfacial friction coefficient of water flow in CNT and graphene nanopores as a function of the pore width calculated using EMD simulations.

NEMD results are obtained under an external acceleration of 1×10^{11} m s^{-2}, which shows excellent agreement with the EMD results. To validate the linear velocity response regime in NEMD, we applied external accelerations in the range 0.5–8×10^{11} m s^{-2} on a 3 nm wide graphene channel (see figure 6(b)). Velocities deviated from the linear regime at accelerations above 2×10^{11} m s^{-2}. This critical acceleration is smaller than the value that we found for a 2.72 nm diameter CNT, for which 4×10^{11} m s^{-2} was still in the linear regime. To probe the linear response, the slip length in graphene channels were calculated both for 1×10^{11} and 4×10^{11} m s^{-2}. With the increasing pore width, the magnitude of L_s remained constant at an acceleration of 1×10^{11} m s^{-2} and we observed a similar trend in slip length using the EMD approach (see figure 7). The results are in excellent agreement with the results of Kannam *et al* [31], who estimated ~60 nm slip length in graphene nanochannels of similar width range. At 4×10^{11} m s^{-2}, L_s shows an

increasing trend with the pore width due to nonlinear effects. Therefore, the limiting slip length for a fluid-solid system can only be estimated from NEMD at accelerations below a critical value (i.e., in the linear response regime), above which L_s is dependent on the magnitude of external acceleration.

3.4. Friction coefficient of water flow in CNT, BNNT and graphene nanopores.

The diameter dependency of L_s in CNTs has been attributed to the curvature-induced variation of the surface potential energy, with the energy landscape becoming extremely smooth in smaller channels [21]. This can be confirmed considering the solid–liquid interfacial friction coefficient, which is related to the relaxation time (see equation (6)). Figure 8 shows a monotonic increase in λ with the tube diameter. The higher slip length in smaller tubes can thus be associated with the lower friction of water on the tube surface. However, in large diameter tubes, the curvature effect on λ is

reduced. The tube diameters considered in our study are not sufficiently large for λ to reach a constant, equivalent to that on a graphene nanopore. An estimate of λ shows no strong dependence on the pore width in graphene-water system, which attributes to the constant slip length. Furthermore, in BNNT, we obtained a very large friction coefficient of water at the solid boundary, which results in low fluid slip.

The friction coefficient can also be calculated from nonequilibrium simulations by calculating the ratio of tangential force (F) exerted by the fluid on the solid to the slip velocity (u_s), $\lambda = F/u_s$. Therefore, λ for a given system can be determined from the slope of a force-velocity graph, obtained from simulations with different external accelerations. However, the computational time required to generate even a single data point in figure 8 using the NEMD method is an order of magnitude higher than for the EMD approach.

4. Conclusion

In this study, we derived and validated an expression to estimate the slip length in cylindrical nanopores from EMD simulations. The approach was validated against NEMD simulation data in systems of water confined in CNTs of different diameters. The EMD and NEMD results showed close agreement across the range of tube diameters and driving forces (in the linear response regime). We observed a monotonic decrement in slip length with an increasing CNT diameter. The slip length dependency on the CNT diameter was due to the curvature-induced variation in friction coefficient. Conversely, the friction of water confined between parallel graphene sheets showed no strong dependency on the channel width, which attributes to the constant slip length observed. The EMD method was also validated for a BNNT-water system, in which a very small slip length was observed. Unlike the plug-like flow in CNT, NEMD analysis of water flow in BNNT showed a deviation from plug velocity profile, with the slip velocity significantly lower than the average fluid velocity. Also for this system, the EMD and NEMD results were in excellent agreement, demonstrating the applicability of the proposed EMD method also for hydrophilic cylindrical nanopores.

These results provide valuable insight into the slip of fluids in cylindrical nanopores. Being able to calculate the slip length from EMD simulations is an important step towards consistency in the literature since the conventional NEMD approach suffers from two main shortcomings. First, NEMD approach relies on extremely large driving forces to collect sufficient statistics. At these large driving forces, the response might become nonlinear, thus deviating from the response that is of experimental interest. An EMD method does not suffer from this limitation since it evaluates the linear response of the system. Furthermore, in narrow hydrophobic pores, the velocity slip on the channel surface is very high, such that the measured slip length is very sensitive to even a minute change in the slope of the NEMD velocity profile close to the tube surface. Our EMD method overcomes these challenges and offers an appealing

alternative in which the slip length for fluids in cylindrical nanopores can be calculated from a single EMD simulation. We believe that the EMD method and the results drawn from it will benefit the design and implementation of future devices in nanotechnology.

ORCID iDs

Sarith P Sathian https://orcid.org/0000-0003-2756-7210

References

[1] Eijkel J C and Van Den Berg A 2005 Nanofluidics: what is it and what can we expect from it? *Microfluid. Nanofluid.* **1** 249–67

[2] Sparreboom W, van den Berg A and Eijkel J C 2009 Principles and applications of nanofluidic transport *Nat. Nanotechnol.* **4** 713

[3] Noy A, Park H G, Fornasiero F, Holt J K, Grigoropoulos C P and Bakajin O 2007 Nanofluidics in carbon nanotubes *Nano Today* **2** 22–9

[4] Batchelor G K 2000 *An Introduction to Fluid Dynamics* (Cambridge: Cambridge University Press)

[5] Hartkamp R, Ghosh A, Weinhart T and Luding S 2012 A study of the anisotropy of stress in a fluid confined in a nanochannel *J. Chem. Phys.* **137** 044711

[6] Hansen J S, Dyre J C, Daivis P, Todd B D and Bruus H 2015 Continuum nanofluidics *Langmuir* **31** 13275–89

[7] Bocquet L and Charlaix E 2010 Nanofluidics, from bulk to interfaces *Chem. Soc. Rev.* **39** 1073–95

[8] Ho T A, Papavassiliou D V, Lee L L and Striolo A 2011 Liquid water can slip on a hydrophilic surface *Proc. Natl Acad. Sci. USA* **108** 16170–5

[9] Maxwell J C V I I 1879 On stresses in rarified gases arising from inequalities of temperature *Phil. Trans. R. Soc.* **170** 231–56

[10] Navier C L 1827 Mémoire sur les lois du mouvement des fluides *Mem. Acad. R. Sci. France* **6** 389–440

[11] Majumder M, Chopra N, Andrews R and Hinds B J 2005 Nanoscale hydrodynamics: enhanced flow in carbon nanotubes *Nature* **438** 44

[12] Holt J K, Park H G, Wang Y, Stadermann M, Artyukhin A B, Grigoropoulos C P, Noy A and Bakajin O 2006 Fast mass transport through sub-2-nanometer carbon nanotubes *Science* **312** 1034–7

[13] Qin X, Yuan Q, Zhao Y, Xie S and Liu Z 2011 Measurement of the rate of water translocation through carbon nanotubes *Nano Lett.* **11** 2173–7

[14] Du F, Qu L, Xia Z, Feng L and Dai L 2011 Membranes of vertically aligned superlong carbon nanotubes *Langmuir* **27** 8437–43

[15] Hummer G, Rasaiah J C and Noworyta J P 2001 Water conduction through the hydrophobic channel of a carbon nanotube *Nature* **414** 188

[16] Kotsalis E, Walther J and Koumoutsakos P 2004 Multiphase water flow inside carbon nanotubes *Int. J. Multiph. Flow* **30** 995–1010

[17] Thomas J A, McGaughey A J H and Kuter-Arnebeck O 2010 Pressure-driven water flow through carbon nanotubes: Insights from molecular dynamics simulation *Int. J. Therm. Sci.* **49** 281–9

[18] Thomas J A and McGaughey A J H 2008 Reassessing fast water transport through carbon nanotubes *Nano Lett.* **8** 2788–93

[19] Thomas J A and McGaughey A J H 2009 Water flow in carbon nanotubes: transition to subcontinuum transport *Phys. Rev. Lett.* **102** 184502

[20] Joseph S and Aluru N 2008 Why are carbon nanotubes fast transporters of water? *Nano Lett.* **8** 452–8

[21] Falk K, Sedlmeier F, Joly L, Netz R R and Bocquet L 2010 Molecular origin of fast water transport in carbon nanotube membranes: superlubricity versus curvature dependent friction *Nano Lett.* **10** 4067–73

[22] Babu J S and Sathian S P 2011 The role of activation energy and reduced viscosity on the enhancement of water flow through carbon nanotubes *J. Chem. Phys.* **134** 194509

[23] Kannam S K, Todd B D, Hansen J S and Daivis P J 2013 How fast does water flow in carbon nanotubes? *J. Chem. Phys.* **138** 094701

[24] Secchi E, Marbach S, Niguès A, Stein D, Siria A and Bocquet L 2016 *Nature* **537** 210

[25] Mattia D and Calabrò F 2012 Explaining high flow rate of water in carbon nanotubes via solid–liquid molecular interactions *Microfluid. Nanofluid.* **13** 125–30

[26] Walther J H, Ritos K, Cruz-Chu E R, Megaridis C M and Koumoutsakos P 2013 Barriers to superfast water transport in carbon nanotube membranes *Nano Lett.* **13** 1910–4

[27] Majumder M and Corry B 2011 Anomalous decline of water transport in covalently modified carbon nanotube membranes *Chem. Commun.* **47** 7683–5

[28] Sam A, Kannam S K, Hartkamp R and Sathian S P 2017 Water flow in carbon nanotubes: the effect of tube flexibility and thermostat *J. Chem. Phys.* **146** 234701

[29] Kassinos S, Walther J, Kotsalis E and Koumoutsakos P 2004 Flow of aqueous solutions in carbon nanotubes *Lect. Notes Comput. Sci.* **39** 215–26

[30] Hanasaki I and Nakatani A 2006 Flow structure of water in carbon nanotubes: Poiseuille type or plug-like? *J. Chem. Phys.* **124** 144708

[31] Kannam S K, Todd B D, Hansen J S and Daivis P J 2012 Slip length of water on graphene: limitations of non-equilibrium molecular dynamics simulations *J. Chem. Phys.* **136** 024705

[32] Bocquet L and Barrat J-L 1994 Hydrodynamic boundary conditions, correlation functions, and Kubo relations for confined fluids *Phys. Rev. E* **49** 3079

[33] Sokhan V P, Nicholson D and Quirke N 2001 Fluid flow in nanopores: an examination of hydrodynamic boundary conditions *J. Chem. Phys.* **115** 3878–87

[34] Sokhan V P, Nicholson D and Quirke N 2002 Fluid flow in nanopores: accurate boundary conditions for carbon nanotubes *J. Chem. Phys.* **117** 8531–9

[35] Chen S, Wang H, Qian T and Sheng P 2015 Determining hydrodynamic boundary conditions from equilibrium fluctuations *Phys. Rev. E* **92** 043007

[36] Kannam S K, Todd B D, Hansen J S and Daivis P J 2011 Slip flow in graphene nanochannels *J. Chem. Phys.* **135** 016313

[37] Kannam S K, Todd B D, Hansen J S and Daivis P J 2012 Interfacial slip friction at a fluid-solid cylindrical boundary *J. Chem. Phys.* **136** 244704

[38] Hansen J S, Todd B D and Daivis P J 2011 Prediction of fluid velocity slip at solid surfaces *Phys. Rev. E* **84** 016313

[39] Sokhan V P and Quirke N 2008 Slip coefficient in nanoscale pore flow *Phys. Rev. E* **78** 015301

[40] Sokhan V P and Quirke N 2004 Interfacial friction and collective diffusion in nanopores *Mol. Simul.* **30** 217–24

[41] Groombridge M, Schneemilch M and Quirke N 2011 Slip boundaries in nanopores *Mol. Simul.* **37** 1023–30

[42] Sokhan V P, Nicholson D and Quirke N 2004 Transport properties of nitrogen in single walled carbon nanotubes *J. Chem. Phys.* **120** 3855–63

[43] Sokhan V P, Quirke N and Greenwood J 2005 Viscous drag forces in gas operated pressure balances *Mol. Simul.* **31** 535–42

[44] Evans D J and Holian B L 1985 The Nose–Hoover thermostat *J. Chem. Phys.* **83** 4069–74

[45] Brenner D W, Shenderova O A, Harrison J A, Stuart S J, Ni B and Sinnott S B 2002 A second-generation reactive empirical bond order (REBO) potential energy expression for hydrocarbons *J. Phys.: Condens. Matter* **14** 783

[46] Mark P and Nilsson L 2001 Structure and dynamics of the TIP3P, SPC, and SPC/E water models at 298 K *J. Phys. Chem. A* **105** 9954–60

[47] Markesteijn A, Hartkamp R, Luding S and Westerweel J 2012 A comparison of the value of viscosity for several water models using Poiseuille flow in a nano-channel *J. Chem. Phys.* **136** 134104

[48] Werder T, Walther J, Jaffe R, Halicioglu T and Koumoutsakos P 2003 On the water- carbon interaction for use in molecular dynamics simulations of graphite and carbon nanotubes *J. Phys. Chem. B* **107** 1345–52

[49] Wolf D, Keblinski P, Phillpot S and Eggebrecht J 1999 Exact method for the simulation of Coulombic systems by spherically truncated, pairwise r- 1 summation *J. Chem. Phys.* **110** 8254–82

[50] Tersoff J 1989 Modeling solid-state chemistry: interatomic potentials for multicomponent systems *Phys. Rev. B* **39** 5566

[51] Rajegowda R, Kannam S K, Hartkamp R and Sathian S P 2018 Thermophoretically driven water droplets on graphene and boron nitride surfaces *Nanotechnology* **29** 215401

[52] Wei X and Luo T 2018 Effects of electrostatic interaction and chirality on the friction coefficient of water flow inside single-walled carbon nanotubes and boron nitride nanotubes *J. Phys. Chem. C* **122** 5131–40

[53] Plimpton S 1995 Fast parallel algorithms for short-range molecular dynamics *J. Comput. Phys.* **117** 1–19

[54] Fanourgakis G S, Medina J S and Prosmiti R 2012 Determining the bulk viscosity of rigid water models *J. Phys. Chem. A* **116** 2564–70

[55] Li T, Gao J, Szoszkiewicz R, Landman U and Riedo E 2007 Structured and viscous water in subnanometer gaps *Phys. Rev. B* **75** 115415

[56] Alexiadis A and Kassinos S 2008 Molecular simulation of water in carbon nanotubes *Chem. Rev.* **108** 5014–34

[57] Nicholls W, Borg M K, Lockerby D A and Reese J 2012 Water transport through carbon nanotubes with defects *Mol. Simul.* **38** 781–5

[58] Krishnan T S, Babu J S and Sathian S P 2013 A molecular dynamics study on the effect of thermostat selection on the physical behavior of water molecules inside single walled carbon nanotubes *J. Mol. Liq.* **188** 42–8

[59] Su J and Guo H 2012 Effect of nanochannel dimension on the transport of water molecules *J. Phys. Chem. B* **116** 5925–32

[60] Ma M, Grey F, Shen L, Urbakh M, Wu S, Liu J Z, Liu Y and Zheng Q 2015 Water transport inside carbon nanotubes mediated by phonon-induced oscillating friction *Nat. Nanotechnol.* **10** 692

[61] Bernardi S, Todd B D and Searles D J 2010 Thermostating highly confined fluids *J. Chem. Phys.* **132** 244706